PERGAMON

International Journal of Heat and Mass Transfer 45 (2002) 3045–3054

International Journal of HEAT and MASS TRANSFER

www.elsevier.com/locate/ijhmt

Shape-factor effect on melting in an elliptic capsule

Sergei A. Fomin [a,*], Alexander V. Wilchinsky [b,1]

[a] *Fracture Research Institute, School of Engineering, Tohoku University, Sendai 980-8579, Japan*
[b] *Institute of Mathematics and Mechanics, Kazan State University, Kazan 420008, Russia*

Received 15 June 2001; received in revised form 16 November 2001

Abstract

An approximate mathematical model of contact melting of an unfixed material in an elliptical capsule is developed. The main characteristic scales and non-dimensional parameters which describe the principal features of the melting process are found. Choosing a special heat flux distribution on the wall of the capsule allows us to derive a closed-form evolution equation for the motion of the solid accounting for the energy convection in the liquid, expressed through the non-linearity of the temperature distribution across the molten layer. It is shown that the melting rate of the solid depends on the shape of the capsule. Generally, elliptical capsules show higher rate of melting than circular ones. Elongated capsules provide more effective melting than oblate ones, even though they have the same aspect ratios and vertical cross-sectional areas. This phenomenon is caused by the fact, that the pressure necessary to support the solid is larger for the elongated capsules than that for oblate ones, which leads to thinning of the molten layer along with the increase of the heat flux across it. The time required for complete melting can be achieved by the right choice of the shape of the capsule, which is specified by the value of the aspect ratio. The found influence of the capsule shape on the melting rate can be used for design and optimization of practical latent-heat–thermal-energy systems.

1. Introduction

Analysis of close-contact melting of a solid in a cavity is motivated by application in latent heat-of-fusion thermal-storage systems. Contact melting in a circular horizontal cylinder has been studied numerically by Saitoh and Hirose [1], analytically and experimentally by Bareiss and Beer [2]. Contact melting in a spherical capsule was investigated numerically by Moore and Bayazitoglu [3] and later, applying the technique proposed in [2], Bahrami and Wang [4], Roy and Sengupta [5] as well as Fomin and Saitoh [6] reported analytical solutions. The general scheme for the scale analysis of the contact melting problem was proposed by Bejan [7]. Although the aforementioned investigations highlight the main characteristics of contact melting inside a capsule, the effect of the shape factor of its cross-section was analysed only for elliptic cylinders [8]. Moreover, a simple linear distribution for the temperature has been assumed, which is acceptable only for very small Stefan numbers. In 1998, Saitoh [9] pointed out that the shape of the capsule is an important factor which should be taken into consideration for optimal design and construction of the latent-heat–thermal-storage systems.

In the present paper the approximate approach developed by Bareiss and Beer [2] is applied with the higher order of accuracy with regard to the temperature distribution for the mathematical modelling of contact melting in a horizontal elliptical cylinder and ellipsoidal capsule. It will be shown, that finding the temperature distribution to the second-order with regard to the Stefan number subject to the temperature distribution on the wall of the capsule, being constant in space, is tantamount to imposing the heat flux on the wall directly proportional to the heat flux at the melting interface. The influence of the shape of the capsule on the melting

* Corresponding author. Tel./fax: +81-22-217-7519.
[1] Present address: Department of Space and Climate Physics, University College London, London, UK.
E-mail address: formin@rift.mech.tohoku.ac.jp (S.A. Fomin).

0017-9310/02/$ - see front matter
PII: S0017-9310(02)00018-2

Nomenclature

a, b	the horizontal and vertical semi-axes of the ellipse
Ar	Archimedes number ($= \rho_l g b^3(\rho_s - \rho_l)/\mu^2$)
$\overline{b}$	the capsule aspect ratio ($= b/a$) ($\overline{b} > 1$ for elongated and $\overline{b} < 1$ for oblate capsules)
c	parameter ($= b^2/a^2 - 1$)
c_s, c_l	the solid and liquid specific heat capacities
g	gravitational acceleration
h	the non-dimensional molten layer thickness
$\overline{h}$	projection of h on the y-direction
k_s, k_l	the solid and liquid heat conductivities
l	the tangential coordinate ($= l^*/a$), as shown in Fig. 1
L_m	the melting latent heat
n	the transverse coordinate ($= n^*/h^*$), as shown in Fig. 1
$\overline{p}$	the liquid pressure
p	the excess liquid pressure ($= (\overline{p}^* - \rho_l g(b - y^*))/p_0$)
Pr	Prandtl number ($= c_l\mu/k_l$)
q_w	the transverse heat flux through the wall of the capsule
$\overline{q}$	constant ($= q_w/\cos\theta$)
Ra	Rayleigh number ($= g\beta\rho_l\rho_s b^3 L_m/(\mu k_l)$)
s	the shift of the reference point fixed in the solid core ($= s^*/2b$)
$\dot{s} = \mathrm{d}s/\mathrm{d}\tau$	melting rate
Ste	Stefan number ($= c_l(T^*_{w0} - T^*_m)/L_m$)
T	the non-dimensional liquid temperature
T^*_m	the dimensional melting temperature
T_w	the non-dimensional wall temperature
T^*_{w0}	the characteristic wall temperature
u, w	dimensionless tangential and transverse velocities
u_t, w_t	scales for the tangential and transverse velocities in the thermal boundary layer along the melting surface on the top of the solid
x	the dimensionless horizontal coordinate ($= x^*/a$)
y	the dimensionless vertical coordinate ($= y^*/b$)

Greek symbols

β	coefficient of thermal expansion
δ	thermal boundary layer thickness
ε	the ratio of the molten layer thickness scale to the capsule semi-axis ($= h_0/a$)
μ	the liquid viscosity
$\nu = 0, 1$	parameter determining if an elliptical cylinder or an ellipsoid of revolution is considered
ρ_s, ρ_l	the densities of the solid and liquid
$\theta = (n, y)$	the angle between the vertical axis and the normal to the capsule wall, as shown in Fig. 1
τ	the non-dimensional time
τ_m	the time required to complete melting of the solid core
τ^r_m	the time of complete melting in scales for a sphere or a circle

Superscript

$*$	dimensional quantity

Subscripts

l	liquid
m	melting
s	solid
w	wall of the capsule
0	scales

rate will be determined with the help of the derived model of melting inside an elliptic capsule of different aspect ratios and supported by physical considerations.

2. System model and analysis

Melting process within an elliptical capsule is illustrated in Fig. 1. The equation $(x^*/a)^2 + (y^*/b)^2 = 1$ describes a generating curve of the surface of the capsule which can be an elliptical cylinder or an ellipsoid of revolution. In the first case (x^*, y^*) are Cartesian coordinates, and in the second case (x^*, y^*) are cylindrical coordinates, where x^* is the radial distance and y^* is the axis of symmetry. Initially, the elliptical capsule contains material in solid phase, which occupies the full space of the capsule. Then the wall temperature is raised to the value $T^*_w > T^*_m$ and is held at this value during the period necessary to melt the solid completely. The unfixed solid bulk sinks [2] because its density is higher than that of the molten liquid. The downward motion of the solid core is characterised by the time-dependent shift s^* of a material-fixed reference point, which is chosen to be the centre of the originally elliptical core. The motion of the solid bulk is accompanied by the generation of liquid at

[2] We do not treat ice.

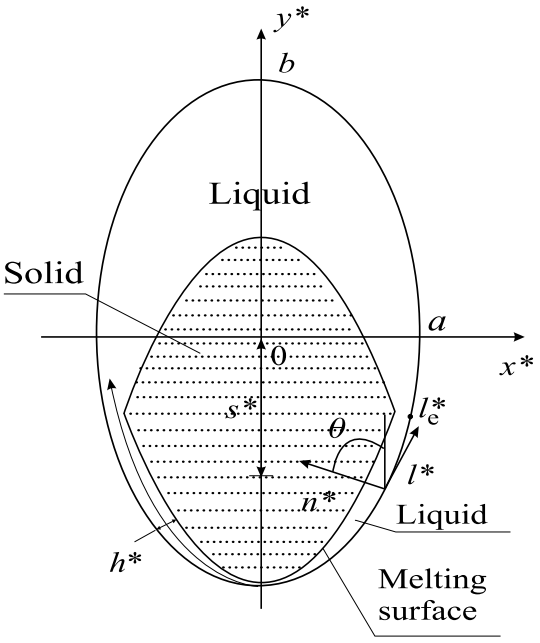

Fig. 1. Close-contact melting inside an elliptic capsule.

the melting surface. This liquid is squeezed up to the space above the solid through a narrow gap between the melting surface and the wall of the capsule. Conventionally, the solid–liquid interface can be divided into two parts by the time dependent value l_e of the tangential coordinate (Fig. 1): the bottom interface ($l < l_e$), which represents the close-contact melting area, where most of the intensive melting occurs, and the upper interface, where much slower "latent" melting takes place. Experiments on melting in a circular horizontal tube conducted by Bareiss and Beer [2] showed that melting at the upper surface of the solid generated approximately 10% of the total melt. Moreover, in these experiments the upper surface of the solid core was very insignificantly changing its shape with time and, therefore, in the model the shape of this surface could be considered as approximately the same throughout the entire process. It was also found that the thickness of the molten layer in the close-contact area is considerably smaller than the characteristic size of the cavity.

The experimentally observed effect of relatively slow melting at the upper surface of the solid can be readily justified by scaling analysis. Obviously, the typical amount of heat transferred to the upper surface of the phase-change material is inversely proportional to the thickness of the thermal boundary layer δ along its surface, while the heat transferred to the melting surface on the bottom of the capsule is inversely proportional to the typical molten layer thickness, h_0. Hence, the heat transferred from the upper surface of the capsule is a small fraction of the order $O(h_0/\delta)$ of the total heat consumed during melting. As a result, the amount of solid melted at the top of the capsule constitutes $O(h_0/\delta)$ part of the total volume of the phase-change material. For the *n*-octadecane contact melting conditions our estimates presented below show that melting of a solid in the upper part of the capsule is 10 times slower than melting on the capsule's bottom. The latter analytical estimate is in a striking consistency with the experimental observations of Bareiss and Beer [2]. Moreover, it will be shown that the influence of the convection in the upper part of the capsule is indifferent to its aspect ratio and can be taken into account by proper re-normalising. The latter confirms that the present model of contact melting in capsules of different aspect ratios has at least the same order of accuracy as previously adopted in the models for the capsules with the circular cross-sections [2–6]. The validation of the above-cited theoretical models by the comparison with the experimental results, available for the circular capsules, simultaneously validates our model as well. This is because the inaccuracy due to the natural convection on the top of the capsule is not affected by the variation of the capsule's aspect ratio, and, therefore, the circular capsules can be taken for the model validation.

The above discussion determines the primary assumptions in modelling of the process under consideration:

1. The relative contribution of the melting at the upper surface of the solid to the whole melting does not depend on the capsule's aspect ratio.
2. The solid core is at the melting point.
3. Thermophysical properties of the materials are constant.
4. The pressure at the upper interface between the solid and liquid is hydrostatic.
5. Since the thickness of the liquid layer in the close-contact area is very small in comparison with the dimensions of the capsule, lubrication approximation can be implemented for mathematical modelling of the heat and mass transfer processes in the molten layer. Therefore, the local two-dimensional curvilinear orthogonal coordinate system (l, n), which is often used in boundary layer problems, is applied as shown in Fig. 1.
6. The motion of the liquid and the solid is non-inertial.

2.1. Governing equations

The curvilinear coordinate system (l^*, n^*) is chosen in such a way that, after normalisation, the transverse coordinate $n = 0$ determines the capsule wall and $n = 1$ determines the solid–liquid interface [10,11]. For the case under consideration we choose the scales as

$$s_0 = 2b, \quad l_0 = a, \quad n_0 = h_0, \quad T_0 = T^*_{w0} - T^*_m,$$
$$p_0 = bg(\rho_s - \rho_l), \quad u_0 = aw_0/h_0.$$

Here, T^*_{w0} is a characteristic temperature of the wall of the capsule. The characteristic excess pressure p_0 is taken as the typical difference between the gravitational and buoyancy forces acting on the solid per unit area of its surface, which must be balanced by the pressure rise over its hydrostatic value in order to keep the solid floating. The other scales will be determined from investigation of the governing equations. Further, we will assume the non-dimensional melting temperature to be zero, $T_m = 0$.

On the basis of assumption (5), the conservation equations of mass, momentum and energy in dimensionless form can be written as

$$\frac{\partial w}{\partial n} + \frac{1}{x^v}\frac{\partial (x^v h u)}{\partial l} = 0, \quad v = 0, 1, \tag{1}$$

$$\frac{\partial p}{\partial l} = \frac{\eta}{h^2}\frac{\partial^2 u}{\partial n^2}, \quad \eta = \frac{\mu u_0 a}{p_0 h_0^2}, \tag{2}$$

$$\frac{\partial p}{\partial n} = 0, \tag{3}$$

$$Ste\left(u\frac{\partial T}{\partial l} + \frac{w}{h}\frac{\partial T}{\partial n}\right) = \frac{1}{h^2}\frac{\partial^2 T}{\partial n^2}, \tag{4}$$

where $v = 0$ identifies the elliptic cylinder and $v = 1$ identifies the ellipsoid of revolution. These are essentially the lubrication equations with an accuracy $O(\varepsilon)$ expressed in curvilinear coordinates. Here the terms of $O(\varepsilon)$ are neglected since the parameter $\varepsilon = h_0/a$, which represents the ratio of the gap-width scale to the characteristic dimension of the capsule, is very small and varies in the range 10^{-3}–10^{-2} for different phase-change materials used in thermal-storage systems. Eq. (1) is the mass balance, (2) and (3) express the longitudinal and normal force balance, and (4) is the steady-state energy balance. To order $O(\varepsilon)$, the Stefan condition at the solid–liquid interface $n = 1$ yields

$$w = \left[\frac{\varphi}{h}\frac{\partial T}{\partial n}\right]_{n=1}, \quad \varphi = \frac{k_l(T^*_{w0} - T^*_m)}{h_0 \rho_l L_m w_0}. \tag{5}$$

To the same order of accuracy, the transverse velocity at the solid–liquid interface $n = 1$ can also be found as

$$w = -\sigma \dot{s}\cos\theta, \quad \sigma = \frac{2\rho_s b}{\rho_l w_0 \tau_0}. \tag{6}$$

From (3) it can be seen that p is a function of only one independent variable l. Equating $\eta = 1$ in (2), $\varphi = 1$ in the Stefan condition (5) and $\sigma = 1$ in (6) yields the scales for the molten layer thickness, transverse velocity and time as follows:

$$h_0^4 = \frac{a^4 Ste\,\bar{b}^2}{ArPr}, \quad w_0 = \frac{k_l(T^*_{w0} - T^*_m)}{\rho_l h_0 L_m}, \quad \tau_0 = \frac{2b\rho_s}{w_0\rho_l}. \tag{7}$$

Because the typical timescale for the solid is $\rho_s c_s a^2/k_s$, assumption (2) requires

$$\frac{\rho_s c_s a^2}{k_s} \ll \frac{2b\rho_s}{w_0\rho_l}. \tag{8}$$

For n-octadecane, $a \geqslant 5$ cm, and the typical temperature difference of 20 °C, we derive for a circular capsule $\varepsilon|_{\bar{b}=1} < 0.0037$.

It should be noted that the adopted scales are valid for capsules with moderate aspect ratios ($\bar{b} = b/a \sim 1$) and for oblate ones $b/a \ll 1$. If the capsule is vertically elongated and $\bar{b} \gg 1$, then instead of a, b should be taken as the spatial scale, and, moreover, $\cos\theta \sim a/b$. The scales in the latter case can be found completely analogously as was done above. For these two cases of strongly elongated and oblate capsules with fixed cross-sectional area $r^2 = ab$ and different scales, we obtain for the elongated capsules

$$\tau_0 \propto \bar{b}^{-7/8}, \quad \bar{b} \geqslant 1, \tag{9}$$

and for oblate ones

$$\tau_0 \propto \bar{b}^{1/8}, \quad \bar{b}^{-1} \geqslant 1. \tag{10}$$

From here it can be seen that, asymptotically, as $\bar{b}^n \to \infty$, where $n = 1$ for elongated capsules and $n = -1$ for oblate ones, the characteristic time of melting for elongated capsules decreases faster than that for oblate ones. This will also be confirmed by computations.

If capsules of different aspect ratios, but the same cross-sectional area are considered, then we have the lubrication approximation accuracy for oblate capsules ($\bar{b} \leqslant 1$)

$$h_0/a = \bar{b}^{1/8}\varepsilon|_{\bar{b}=1} \tag{11}$$

and for elongated ones ($\bar{b} \geqslant 1$)

$$h_0/b = \bar{b}^{-3/8}\varepsilon|_{\bar{b}=1}. \tag{12}$$

This means that the accuracy of the lubrication approximation for the flow in the region where the close-contact melting takes place increases for both capsules.

In order to estimate the general accuracy of the model, the effect of natural convection on the melting at the upper surface of the solid must be taken into account. This effect can be estimated in considering the thin thermal boundary layer of the relatively cold melt generated on the inclined upper surface of the solid core, which flows down governed by the friction – buoyancy balance [1–3]. The heat flux at the upper surface of the solid core can be estimated as $k_l(T^*_{w0} - T^*_m)/\delta$. The dimension of the boundary layer thickness for the elongated capsule is determined by scaling analysis [12] of

the mass, momentum equations and the Stefan condition: $w_t \approx \delta u_t/b$, $\mu u_t/\delta^2 \approx \rho_l g\beta(T^*_{w0} - T^*_m)$ and $k_l(T^*_{w0} - T^*_m)/\delta \approx \rho_s w_t L_m$, where w_t and u_t are scales for the transverse and longitudinal velocities in the thermal boundary layer on the top of the melting solid. The above equations yield $\delta/b \approx Ra^{-1/4}$, where $Ra = g\beta\rho_l\rho_s \times b^3 L_m/(\mu k_l)$. For oblate capsules, the analysis is analogous, however, a must be used as the longitudinal scale, while $\bar{b}g$ is the gravity force projection along the layer. Considering capsules of different aspect ratios, but the same volume ($r^2 = ab = \text{const.}$) as before, and taking into account Eqs. (11) and (12) and that $b = r\bar{b}^{1/2}$, the relative contribution of the melting at the upper surface for oblate and elongated capsules can be finally assessed as

$$\frac{h_0}{\delta} = (Ra^{1/4}\varepsilon)|_{\bar{b}=1}. \tag{13}$$

The above relationship does not depend on the capsule's aspect ratio. This is because an increase of the aspect ratio of the capsules leads to the simultaneously equal increase of the thickness of the boundary layers beneath the solid and above it. The rate of this increase with regard to variation of the aspect ratio, however, is larger for the oblate capsule and, therefore, its melting rate is lower than that of the elongated one. This means that in studying the shape-factor effect on the melting rate of capsules, it is possible to compare melting rates of capsules with the same volume, neglecting the melting at the upper surface, which then can be taking into account simply by increasing the melting rate by the factor of $1 + (Ra^{1/4}\varepsilon)|_{\bar{b}=1}$. For n-octadecane melting conditions $\rho_l = 770$ kg/m^3, $\rho_s = 884$ kg/m^3, $\mu = 3 \times 10^{-3}$ s N/m^2, $c_l = 1.6$ kJ/kg K, $k_l = 0.15$ W/m K, $L_m = 240$ kJ/kg, $T^*_{w0} - T^*_m = 20$ °C, $\beta = 10^{-3}$ K^{-1} and $r = 0.05$ m, we have $(Ra^{1/4}\varepsilon)|_{\bar{b}=1} = 0.095$. Therefore for this particular case, the effect of the melting at the upper surface is about 10% of the close-contact melting. It is gratifying to see that the latter estimate is in exact agreement with experimental data available in [2,3].

Balancing the forces acting on the solid in the vertical direction, namely the gravitational force and the force exerted by the liquid, yields with an accuracy of $O(\varepsilon)$:

$$\int_0^{\sqrt{1-s^2}} px^\nu \,\mathrm{d}x = F_\nu(s), \quad \nu = 1, 0, \tag{14}$$

where

$$F_0 = (\arccos s - s\sqrt{1-s^2}), \quad F_1 = \frac{2}{3} - s + \frac{s^3}{3}. \tag{15}$$

The magnitude of the gravitational force at the RHS of Eq. (14) depends on the solid bulk volume which varies with time since s is a function of time. As it can be seen from Eqs. (15), in the final stage of the melting process when s tends to 1, the volume of the solid bulk and, therefore, the magnitude of the gravitational force vanish to zero. At the LHS of Eq. (14), the force acting in the direction opposite to the gravitational force is represented by the force of pressure in the liquid layer. The other component of this force caused by the shear stresses is ignored since its magnitude is of order $O(\varepsilon)$.

2.2. Evolution equation for the solid motion

Integrating Eq. (2) twice with respect to n and taking into account the no-slip conditions on both the capsule wall and melting interface yields

$$u = \frac{h^2}{2}\frac{\partial p}{\partial l}(n^2 - n). \tag{16}$$

Substituting Eq. (16) into the continuity equation (1), integrating with respect to n and l, and taking into account (6) and the impermeability condition on the wall of the capsule, we derive the expressions for the pressure gradient and the transverse velocity

$$\frac{\partial p}{\partial l} = -\frac{12x\dot{s}}{(\nu+1)h^3}, \tag{17}$$

$$w = \dot{s}\cos\theta(2n^3 - 3n^2). \tag{18}$$

Using the expression for the pressure gradient (17) we can write the force balance equation (14) in the form

$$\frac{12\dot{s}}{(\nu+1)^2}\int_0^{\sqrt{1-s^2}} \frac{x^{\nu+2}}{h^3\cos\theta}\,\mathrm{d}x = F_\nu \quad (\nu = 0, 1), \tag{19}$$

where F_0 and F_1 are determined by Eq. (15). Integrating the energy equation (4) with respect to n in the interval $(0, 1)$ and using the mass conservation equation (1) and the Stefan condition (5), we derive the energy balance equation in the integral form

$$\frac{Ste}{x^\nu}\frac{\partial}{\partial l}\left(hx^\nu\int_0^1 uT\,\mathrm{d}n\right) = q_w - \dot{s}\cos\theta, \tag{20}$$

where $q_w = q_w(l)$ is the transverse heat flux at the wall of the capsule.

2.3. Simplified model of close-contact melting

As it was already mentioned, the derivation of the mathematical model presented above is based on the fact that the parameter $\varepsilon = h_0/a \sim 10^{-3}$–$10^{-2}$, therefore values of order $O(\varepsilon)$ are ignored. This model is governed by another small parameter – the Stefan number. For a number of situations and a variety of phase-change materials $Ste < 0.5$. The latter allows us to implement the perturbation methods and to neglect in the further analysis the terms of the order of $O(Ste^2)$. Within the bounds of the adopted accuracy, the temperature

profile, which should be substituted into the LHS of Eq. (20), can be taken as follows:

$$T = T_w(1-n) + O(Ste). \tag{21}$$

From the Stefan condition (5) and Eq. (21) it also follows that

$$T_w = h\dot{s}\cos\theta + O(Ste). \tag{22}$$

Substituting the expression for tangential velocity (16) and the linear temperature profile across the molten layer (21) into the LHS of the energy balance equation (20), where the pressure gradient $\partial p/\partial l$ and the wall temperature T_w are defined by Eqs. (17) and (22), respectively, after integration over l we derive, with an accuracy of $O(Ste^2)$,

$$Ste\,h\dot{s}\cos\theta = 2\left(\frac{v+1}{\dot{s}x^{v+1}}\int_0^l x^v q_w\,dl - 1\right). \tag{23}$$

If the heat flux distribution on the wall of the capsule, $q_w = q_w(l)$, is given, then (23) and the force balance equation (19) constitute an integro-differential system, from which the shift of the solid core, $s = s(\tau)$, and the thickness of the molten layer, $h = h(l,\tau)$, can be determined. For an arbitrary q_w, this system of equations can be solved numerically, however, the closed-form analytical solution can be readily obtained, provided that on the wall of the capsule the special heat flux distribution is assumed as $q_w = \bar{q}\cos\theta$, where $\bar{q}$ does not depend on l, and $\cos\theta = dx/dl = \sqrt{1-x^2}/\sqrt{1+cx^2}$. Evidently, because the heat flux at the melting interface is equal to $\dot{s}\cos\theta$, the adopted heat flux at the wall is proportional to that at the melting interface. As is shown below, this assumption leads to the uniform temperature on the capsule's wall, which is physically feasible [6] and has been widely used in the previous research [1–5].

For the adopted form of the heat flux at the wall, Eq. (23) converts to

$$\bar{h} = \frac{2(\bar{q}-\dot{s})}{Ste\,\dot{s}^2}, \quad \bar{h} = h\cos\theta, \tag{24}$$

from which it follows that the product $\bar{h} = h\cos\theta$ does not depend on x and can be a function of the time only. As a result the force balance equation (19) reduces to

$$\bar{h}^3 = \frac{12\dot{s}}{(v+1)^2 F_v}\int_0^{\sqrt{1-s^2}} x^{v+2}\left(\frac{dx}{dl}\right)^2 dx \tag{25}$$

and the pressure distribution can be found from (17) as

$$p = \begin{cases} \frac{3\dot{s}}{(v+1)\bar{h}^3}\left[(1-x^2)^2 - s^4\right], & c = 0, \\ \frac{6\dot{s}}{(v+1)\bar{h}^3}\left[\left(\frac{1}{c}+\frac{1}{c^2}\right)\ln\frac{1+c(1-s^2)}{1+cx^2} - \frac{1-s^2-x^2}{c}\right], & c \neq 0. \end{cases} \tag{26}$$

For the case under consideration, the boundary conditions at the solid–liquid interface (5) and $T_m = 0$ do not depend on l. Therefore, we can suppose that for the specified case the liquid temperature is a function of n only, which will be confirmed by the found solution. Basing on this assumption we reduce the energy equation (4) by ignoring the first term on the left-hand side. Then, substituting expression (18) for w into (4) yields

$$Ste\,\bar{h}\dot{s}(2n^3 - 3n^2)\frac{\partial T}{\partial n} = \frac{\partial^2 T}{\partial n^2}. \tag{27}$$

Because (27) does not include coefficients depending on l, the temperature T will be a function of n only and the wall of the capsule is isothermal. The temperature distribution therefore can be readily found to order of $O(Ste^2)$

$$T = \bar{h}\dot{s}\left[1 - n + Ste\,\bar{h}\dot{s}\left(\frac{7}{20} - \frac{n^5}{10} + \frac{n^4}{4} - \frac{n}{2}\right)\right]. \tag{28}$$

For the wall temperature, $T|_{n=0} = T_w$, after some simple manipulations and ignoring the terms of $O(Ste^2)$, this formula gives

$$\bar{h}\dot{s} = T_w(1 - 7Ste\,T_w/20), \tag{29}$$

which, together with (24), determines $\bar{q}$ through the wall temperature

$$\bar{q} = \dot{s}\left[1 + \frac{1}{2}Ste\,T_w(1 - 7Ste\,T_w/20)\right]. \tag{30}$$

From (29) it is clear, that the adopted form of the heat flux at the wall, $q_w = \bar{q}\cos\theta$, linearly proportional to the heat flux at the melting surface, determines the wall temperature, constant along the wall, and enables us to find the temperature distribution to order $O(Ste^2)$.

Substituting Eq. (29) into the force balance equation (25) leads to the equation for the downward velocity of the solid bulk $ds/d\tau$

$$\dot{s} = \left[(v+1)^2 F_v T_w^3(1 - 7Ste\,T_w/20)^3/12G_v\right]^{1/4}, \tag{31}$$

where for $v = 0$

$$G_0 = \begin{cases} (2+3s^2)(1-s^2)^{3/2}/15, & c = 0, \\ \frac{-(1-s^2)^{3/2}}{3c} + \left(\frac{1}{c}+\frac{1}{c^2}\right)\left(\sqrt{1-s^2} - \frac{\arctan\sqrt{c(1-s^2)}}{\sqrt{c}}\right), & c > 0, \\ \frac{-(1-s^2)^{3/2}}{3c} + \left(\frac{1}{c}+\frac{1}{c^2}\right)\left(\sqrt{1-s^2} - \frac{\operatorname{arth}\sqrt{-c(1-s^2)}}{\sqrt{-c}}\right), & c < 0 \end{cases}$$

and for $v = 1$

$$G_1 = \begin{cases} (1+2s^2)(1-s^2)^2/12, & c = 0, \\ -\frac{(1-s^2)^2}{4c} + \frac{(1+c)(1-s^2)}{2c^2} - \frac{1+c}{2c^3}\ln[1+c(1-s^2)], & c \neq 0. \end{cases}$$

Eq. (31) includes only two dimensionless parameters. Parameter $c = (b/a)^2 - 1$ depends on the aspect ratio b/a of the ellipse and the Stefan number characterises the effect of the material properties and wall temperature. If the wall temperature is constant also with regard to time, then because the functions F and G depend only on s and c, we can eliminate the factor at the RHS of (31) depending on T_w and Ste by rescaling the time τ

$$\tilde{\tau} = \tau[(v+1)^2 T_w^3 (1 - 7Ste\, T_w/20)^3/12]^{1/4} \tag{32}$$

to derive in new variables

$$\mathrm{d}s/\mathrm{d}\tilde{\tau} = [F_v/G_v]^{1/4}. \tag{33}$$

Therefore, the knowledge of the function $s(\tilde{\tau}, c)$ when b/a is fixed permits us to find solution of the problem for all quantities of the cross-sectional area of the ellipse, wall temperature and material properties. On the other hand, if then function s^* and the time of complete melting τ_m^* are found from natural experiments on melting of any particular material in an elliptical capsule of fixed aspect ratio and arbitrary cross-sectional area, then s^* and τ_m^* can be readily obtained for any other material, wall temperature, cross-sectional area and the same ellipse aspect ratio by means of scale transformation.

Let us consider a different situation, when the ellipse cross-sectional area $r^2 = ab$ and the Stefan number are fixed, whereas the aspect ratio is changed. Considering two cases of melting of the same material induced by the same wall temperature inside the capsules with different ellipse aspect ratios, which are denoted by subscripts 1, 2, we have $\tau_{m1}^*/\tau_{m2}^* = (\bar{b}_1/\bar{b}_2)^{1/8}\tilde{\tau}_{m1}/\tilde{\tau}_{m2}$, where $\tilde{\tau}_m$ depends only on the aspect ratio of the ellipse. Hence, the ratio of dimensional times required for complete melting is affected only by the values of the aspect ratios and does not depend on the cross-sectional area of the capsule, material properties and wall temperature.

Since the LHS of Eq. (27) is a value of $O(Ste)$ and the parameter Ste is small, the heat transport between the solid and the capsule wall is dominated by conduction in the transverse direction. Because the developed model accounts for the heat convection due to the adopted form of the heat flux on the wall, which enables us to find the temperature distribution to order of $O(Ste^2)$, it is advantageous to introduce the Nusselt number, in order to describe the effect of the heat convection in the molten layer on the heat transfer across it. The Nusselt numbers at the wall of the capsule, Nu_w, and at the melting interface, Nu_m can be defined as

$$Nu_w = \frac{1}{T|_{n=1} - T_w}\left.\frac{\partial T}{\partial n}\right|_{n=0}, \qquad Nu_m = \frac{1}{T|_{n=1} - T_w}\left.\frac{\partial T}{\partial n}\right|_{n=1}. \tag{34}$$

Taking into account the temperature distribution (28) and neglecting the terms of order Ste^2, we derive

$$Nu_w = 1 + \frac{3}{20}Ste\, T_w, \quad Nu_m = 1 - \frac{7}{20}Ste\, T_w. \tag{35}$$

For $Ste = 0.1$, we have corrections of 1.5% and 3.5%, respectively, which means that in this case the heat flux at the wall can be satisfactorily approximated by the linear interpolation of the temperature distribution. Mathematically it means that, in this case, the convection term at the RHS of Eq. (4) can be neglected. For larger values of the Stefan number, however, the linear approximation will be too rough, and the corrections are necessary to include. Because the developed model determines the temperature distribution to order of $O(Ste^2)$ accounting for the convection, it can accurately describe contact melting processes characterised by relatively large Stefan numbers, say $Ste < 0.4$.

3. Results and discussion

Among the different phase-change materials used in the thermal energy storage systems, *n*-octadecane is most frequently used. Physical properties of this material are well documented. Even though numerical computations provided below are for *n*-octadecane melting conditions, general conclusions can be drawn. On the basis of the closed-form solution obtained above, the main values characterising the process of contact melting, such as the pressure, time of melting and melting rate can be easily calculated.

Because, as can be seen from (26), the pressure profile with regard to x depends only on x and s, while the other parameters effect only its amplitude, in Fig. 2 we present the normalised pressure distribution only for the elliptic cylinder. Even though the pressure at the bottom of the elongated capsule ($\bar{b} > 1$) is higher than in the case of circular or oblate ones, it is characterised by higher non-uniformity of distribution than the others. While the pressure gradient for the oblate capsule is a monotone function, changing from zero at the centre of the bottom to its highest value at the marginal point, $x = x_{max}$, the pressure gradient for the elongated capsule is non-monotone, which is determined by the existence of a point of inflexion of the curve. The inflexion becomes stronger as $s \to 0$. Such a difference in the behaviour is caused by the difference between the typical slopes of the capsule walls: for very oblate capsules the wall is almost horizontal, and the pressure, supporting the solid afloat, is distributed uniformly with regard to x; for highly elongated capsules the wall is close to vertical, and the pressure, necessary to support the solid, is concentrated in the small region, where the wall slope is still gentle – near the vertical principal axis. Supporting the solid at higher slopes of the contact surface would require much

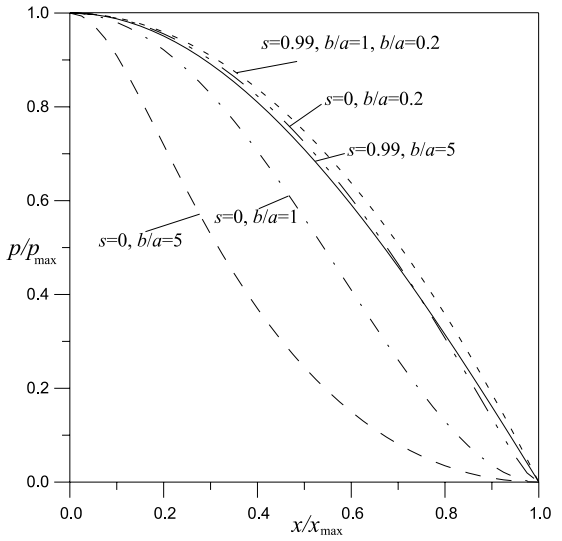

Fig. 2. The normalised pressure distribution with regard to x for different ellipse aspect ratios, $\bar{b} = b/a$, at the beginning ($s = 0$) and end ($s = 0.99$) of melting. At the end of the melting ($s = 0.99$), the normalised pressure distribution for the circular ($b/a = 1$) and oblate ($b/a = 0.2$) capsules differs insignificantly, therefore it is presented by one curve.

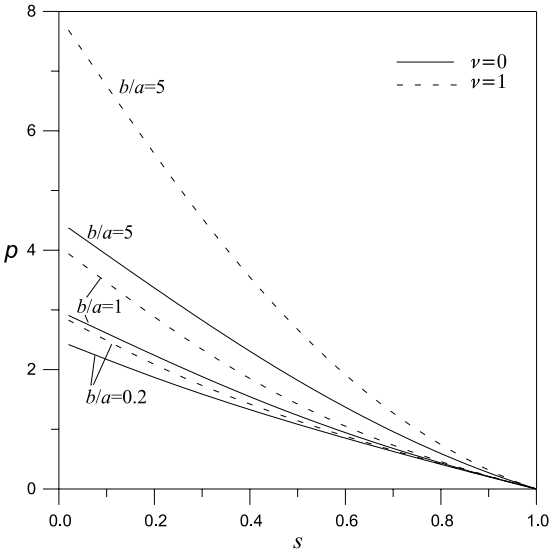

Fig. 3. Variation of the pressure at the bottom ($x = 0$) during the melting process for the capsules with different aspect ratios. $\nu = 0$ for the elliptic cylinders, and $\nu = 1$ for the ellipsoids of revolution.

higher pressure there, which would lead to a negative pressure gradient along the wall, hampering the melt outflow. This explanation is also supported by the weakening of the peculiarity as $s \to 1$, namely, when the width of the solid becomes smaller, and its mean surface slope becomes more gentle. Moreover, because $h = \bar{h}/\cos\theta$, and $\bar{h} = \text{const}$, we have $h \sim 1/\cos\theta$. For moderate x, $\cos\theta \sim a/b \ll 1$, while $\cos\theta \sim 1$ when $x \sim a/b$. Therefore, in a small region around the vertical semi-axis with the typical length a/b, the molten layer thickness sharply decreases, which leads to the sharp increase of the pressure.

The pressure variation at the bottom of the capsule, $x = 0$, during melting is presented in Fig. 3. As it can be expected, the pressure decreases with time from its maximal, initial, value, when $s = 0$ up to zero at the final stage, when $s = 1$. [3] Moreover, the pressure for the ellipsoid of revolution is higher than that for the cylinder of the same area of vertical cross-section, because as $x \to 0$, the area of the horizontal cross-section at $y = \bar{b}(1-x)^{1/2}$ tends to zero as x^2 for the ellipsoid of revolution, and x for the elliptic cylinder, while the pressure exerted on these areas must support the same mass of the solids.

Variation of the melting rate during the melting is shown in Fig. 4. It can be seen that the melting rate of the ellipsoid of revolution is higher than that of the elliptic cylinder, which is caused, firstly, by the smaller molten-layer thickness caused, in turn, by higher pressure, as was shown above, and, secondly, by the larger area of contact melting due to the closed form of its surface. Another feature of the process is that for the oblate capsules the melting rate changes slowly during the melting, while for the elongated ones, the melting rate decreases much faster. This can be explained by the following. As was shown in Fig. 2, for the elongated capsules the pressure is concentrated in a small region near the vertical semi-axis, while for the oblate ones it is distributed much more homogeneously. Therefore, during the melting the solid mass in the elongated capsule decreases while the main region of the pressure remains the same, which leads to the pressure drop and the slowing of the melting. In case of the oblate capsules, the solid mass decreases together with the main region of the pressure, therefore, the change of the melting rate during the melting is much less pronounced.

In order to estimate the effect of the shape factor on the effectiveness of melting it is reasonable to consider capsules of the same cross-sectional area, which means that the quantity $r^2 = ab$ is fixed. Since the adopted scales depend on a and b, we present results of computations for different a and b using the scales obtained above when $a = b = r$, which corresponds to a circular

[3] It should be noted that in Figs. 3 and 4 the curves corresponding to different values of $\bar{b}$ are obtained using different scales, because these scales depend on a and b. However, for the same values of a and b, the scales do not differ if the capsule is an elliptic cylinder or an ellipsoid of revolution.

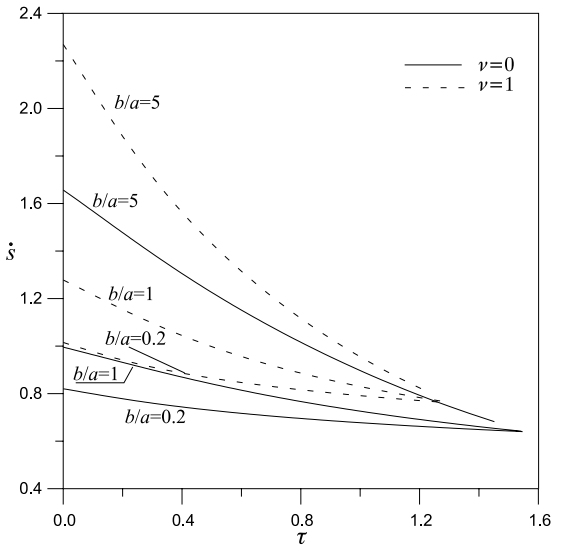

Fig. 4. Variation of the melting rate, $ds/d\tau$, with time for the capsules with different aspect ratios.

cylinder or a sphere. We will denote the time of complete melting in these variables by τ_m^r. Fig. 5 shows how the complete time of melting varies with the aspect ratio $(b/a)^n$. For the elongated capsules the exponent $n = 1$ and the aspect-ratio $b/a > 1$, for the oblate capsules $n = -1$ and, hence, the aspect ratio $b/a < 1$. As can be seen, the elliptical capsules with large aspect ratios show higher rate of melting than the circular ones, and the elongated capsules are characterised by higher rate of melting than the oblate ones (which also follows from the scaling analysis (9), (10)), therefore the aspect ratio b/a can be used as a control parameter for the time of melting. The time required for complete melting can be achieved by the right choice of the shape of the capsule, which is specified by the value of the aspect ratio.

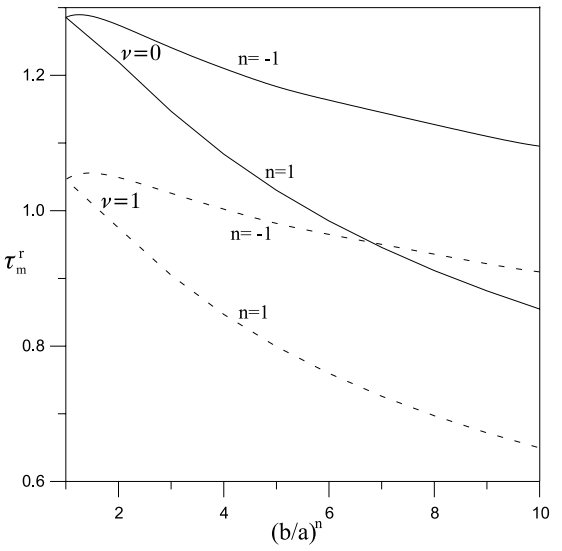

Fig. 5. Variation of the time of complete melting inside the elliptical capsules of the same cross-sectional area vs the ellipse aspect ratio.

However, it is interesting to note, that the maximal time of melting is achieved when $b/a = 0.8$, but not when the capsule is circular, $b/a = 1$. This can be explained by the existence of two mechanisms influencing the effectiveness of the melting. Firstly, as the aspect ratio increases, the area of contact melting also increases, which leads to the higher effectiveness of the melting. On the other hand, the effectiveness of the melting depends also on the thickness of the molten layer, which is thinner for elongated capsules than for oblate ones, due to the larger pressure, exerted by the liquid on the solid. Therefore, when the aspect ratio of an oblate capsule increases, these two mechanisms counteract, which, for moderate aspect ratios, leads to prevailing of the second one, as is demonstrated by the increase of the complete melting time for $\bar{b} < 0.8$. The mechanisms balance each other at $\bar{b} = 0.8$, and when the aspect ratio increases further, the first mechanism prevails. This counteraction leads to lower effectiveness of melting for oblate capsules, which was also determined by the scaling analysis (9) and (10), performed for large aspect ratios.

As it was already mentioned, the present calculations are carried out for the typical n-octadecane melting conditions; in this case Stefan number $Ste \approx 0.1$. Hence, according to Eq. (31), if the forced convection along the gap between the capsule wall and melting surface in the close-contact melting area is ignored (assuming in (31) parameter $Ste = 0$), then it would result in approximately 3.5% exaggeration of the melting rate. For other phase-change materials and melting conditions, when Stefan number becomes larger, the effect of the forced convection on the melting rate would be proportionally stronger.

4. Conclusions

The analysis presented in this paper allowed us to find a closed-form solution describing motion of a melting solid inside elliptic cylinders and ellipsoids of revolution. The temperature distribution is found to order $O(Ste^2)$, which yields the correction $7Ste/20$ to its linear approximation, caused by accounting for the convective heat transfer in the molten layer.

The scaling analysis and numerical calculations showed that the melting rate of solids in elliptic capsules is effected by their aspect ratios. Generally, the melting rate is higher for elongated capsules than for oblate ones, which is caused by the smaller thickness of the

molten layer due to the higher pressure exerted by the solid. In the first case, the pressure, supporting the solid afloat, is concentrated in a small region near the vertical semi-axis, where the surface slope is still gentle, while, for oblate capsules, the pressure is distributed relatively uniformly over the solid surface. This feature is also responsible for fast decrease in time of the melting rate for the elongated capsules in comparison with that for the oblate ones.

Such qualitative conclusions on the influence of the aspect ratio and shape of the capsules on the melting rate can be applied not only to melting in elliptic capsules but also in capsules with other anisotropic forms. A necessary melting rate can be achieved by choosing specific form of the capsule.

Acknowledgements

We are grateful to both referees for remarks, which helped us to improve the work. Alexander Wilchinsky acknowledges financial support of the Russian Academy of Sciences.

References

[1] T. Saitoh, K. Hirose, High Raleigh numbers solutions to problems of latent heat thermal energy storage in a horizontal cylinder capsule, ASME J. Heat Transfer 104 (1982) 545–553.
[2] M. Bareiss, H. Beer, An analytical solution of the heat transfer process during melting of an unfixed solid phase change material inside a horizontal tube, Int. J. Heat Mass Transfer 27 (1984) 739–746.
[3] F. Moore, Y. Bayazitoglu, Melting within a spherical enclosure, ASME J. Heat Transfer 104 (1982) 19–23.
[4] P.A. Bahrami, T.G. Wang, Analysis of gravity and conduction driven melting in a sphere, ASME J. Heat Transfer 109 (1987) 806–809.
[5] S.K. Roy, S. Sengupta, The melting process within spherical enclosure, ASME J. Heat Transfer 109 (1987) 460–462.
[6] S.A. Fomin, T.S. Saitoh, Melting inside a spherical capsule with non-isothermal wall, Int. J. Heat Mass Transfer 42 (1999) 4197–4205.
[7] A. Bejan, Single correlation for theoretical contact melting results in various geometries, Int. Commun. Heat Mass Transfer 19 (1992) 473–483.
[8] S.A. Fomin, A.V. Wilchinsky, T.S. Saitoh, Close-contact melting inside an elliptic cylinder, J. Solar Energy Eng. 122 (4) (2000) 192–195.
[9] T.S. Saitoh, Japanese Patent No. 2755422, 1998.
[10] S.A. Fomin, Mathematical model of heat and mass transfer processes in contact melting, J. Sov. Math. 61 (6) (1992) 2426–2438.
[11] S.A. Fomin, P.S. Wei, V.A. Chugunov, Contact melting by non-isothermal heating surface of arbitrary shape, Int. J. Heat Mass Transfer 38 (17) (1995) 3275–3284.
[12] A. Bejan, Convection Heat Transfer, Wiley, New York, 1984, pp. 109–151.